

# Sequential Bayesian inference with correlated heavy-ion datasets

Lipei Du<sup>a,b</sup>

<sup>a</sup>Department of Physics, University of California, Berkeley, 94270, CA, USA

<sup>b</sup>Nuclear Science Division, Lawrence Berkeley National Laboratory, Berkeley, 94270, CA, USA

---

## Abstract

Bayesian inference provides a natural framework for updating knowledge as new information becomes available, often in a sequential manner by incorporating datasets in stages or reusing previous posteriors as priors. In practice, this is commonly implemented using a factorized update in which datasets are treated as conditionally independent. When datasets are statistically correlated, however, this approximation becomes inconsistent with the joint likelihood and can lead to biased posterior estimates. In this work, we investigate this issue in a controlled setting using pseudo-data with a tunable covariance structure. We compare joint inference, factorized sequential updating, and a formulation based on the exact conditional likelihood. We show that factorized updates reproduce the joint posterior only in the limit of conditional independence, and otherwise lead to systematic deviations that grow with the correlation strength, while conditional updates remain consistent with the joint result. To interpret these deviations, we introduce an information decomposition that separates contributions into components that are new and components that are redundant across datasets. We show that correlations induce a structured, parameter-dependent redistribution of information, governed by the overlap of dataset sensitivities. The resulting mismatch between marginal and conditional information quantitatively explains the observed deviations. These results provide a practical diagnostic for assessing the consistency of sequential Bayesian inference with correlated datasets and highlight the need for a consistent treatment of correlations within a common probabilistic framework.

*Keywords:* Bayesian inference, sequential updating, correlated datasets, conditional likelihood, statistical methods

---

## 1. Introduction

Bayesian inference has become a central framework for quantitative parameter estimation in complex physical systems [1–3]. In relativistic heavy-ion collisions, it is widely used to extract properties of the quark–gluon plasma by confronting multi-observable datasets with dynamical models [4–15]. More broadly, Bayesian methods provide a systematic way to update prior knowledge as new information becomes available, making them a natural language for cumulative scientific inference [16–18].

In many applications, information is acquired in stages. New datasets may become available over time, or previous analyses may provide posterior distributions that serve as inputs to subsequent studies [19, 20]. This motivates the idea of *sequential Bayesian inference*, in which knowledge is progressively refined as additional data are incorporated. Such an approach is attractive in large-scale calibration problems, as it enables modular combination of heterogeneous constraints and facilitates the propagation of prior information across different stages of analysis.

A key question in this context is whether sequential updates remain consistent with joint inference when multiple datasets are combined. In practice, such updates are often carried out by incorporating datasets in stages or by reusing posterior distributions from previous analyses as effective priors. This is

commonly accompanied by treating the individual datasets as conditionally independent, so that the likelihood is taken to factorize into a product of marginal terms [21]. While this approximation simplifies the analysis, it is not always made explicit and its validity depends on the statistical independence of the datasets.

In realistic applications, this assumption is rarely satisfied. Different datasets are often correlated due to shared experimental systematics, common model uncertainties, or underlying physical mechanisms that couple multiple observables [12–14]. In heavy-ion collisions, for example, particle yields, transverse-momentum spectra, and anisotropic flow coefficients are all influenced by common features of the initial state and medium response [22–27]. More generally, correlated constraints arise whenever different measurements probe overlapping aspects of a system [28–33].

When such correlations are present, the likelihood no longer factorizes, and sequential updates based on marginal likelihoods do not, in general, reproduce the result of a joint analysis. This leads to a fundamental inconsistency: factorized sequential inference can yield posterior distributions that differ systematically from those obtained from the full joint likelihood. While effort has been devoted to representing and propagating complex prior information across inference stages [21, 34], the role of statistical correlations between datasets in sequential inference has received comparatively less systematic attention. This is particularly relevant since, even in joint analyses, cross-dataset correlations can be challenging to fully quantify and are

---

*Email address:* ldu2@lbl.gov (Lipei Du)

often treated approximately in practice [12–14, 35], so that their impact may already be nontrivial at the level of the full likelihood.

The purpose of this work is to clarify the role of correlations in sequential Bayesian inference in a controlled and transparent setting. Rather than focusing on a specific phenomenological application, we construct a reduced model that captures the essential statistical structure of multi-observable inference problems, and generate pseudo-data with a tunable covariance matrix that allows the strength of cross-dataset correlations to be varied continuously.

Within this framework, we compare joint inference using the full likelihood, factorized sequential updating, and a formulation based on the exact conditional likelihood. This setup enables a direct and model-independent assessment of how correlations affect posterior inference. We show that factorized updates reproduce the joint posterior only in the limit of conditional independence, and otherwise lead to systematic deviations that grow with the correlation strength. In contrast, conditional sequential updating remains fully consistent with the joint posterior for Gaussian likelihoods and is independent of update order.

Beyond this comparison, we introduce a quantitative framework to analyze how correlations redistribute information between datasets. By decomposing the information content into components that are genuinely new and components that are redundant across datasets, we show that the impact of correlations is strongly parameter-dependent, reflecting the interplay between covariance structure and parameter sensitivities. This provides a direct link between the data covariance, the geometry of parameter constraints, and the resulting deviations in posterior inference.

The remainder of this paper is organized as follows. In Section 2, we introduce the reduced model and pseudo-data construction. In Section 3, we review the Bayesian inference framework and formulate the different sequential updating strategies. In Section 4, we analyze the sensitivity structure, develop an information-theoretic decomposition of correlated datasets, examine the resulting posterior distortions, and quantify their magnitude using the Kullback–Leibler divergence. Finally, Section 5 summarizes the main findings and discusses their broader implications.

## 2. Reduced model and pseudo-data setup

To study the role of correlations in a controlled setting, we consider a reduced model that captures the essential structure of multi-observable inference problems [10, 15, 28]. The model is designed to isolate, in a minimal and transparent way, how different classes of observables constrain overlapping parameter directions. Details of the construction are provided in Appendix A.

We introduce four model parameters,

$$\theta = (S, \varepsilon_2, \kappa_N, \kappa_v), \quad (1)$$

where  $S$  denotes an entropy-like scale,  $\varepsilon_2$  an eccentricity-like parameter, and  $\kappa_N$  and  $\kappa_v$  characterize the response of yield-like

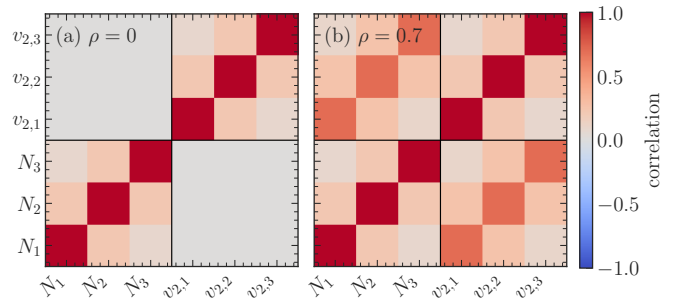


Figure 1: Correlation matrices for the pseudo-data at two representative values of the cross-dataset correlation strength  $\rho$ . The observable ordering is  $(N_1, N_2, N_3, v_{2,1}, v_{2,2}, v_{2,3})$ , with guide lines separating the two observable groups.

and flow-like observables, respectively. The observable vector consists of two groups,

$$d = (N_1, N_2, N_3, v_{2,1}, v_{2,2}, v_{2,3}), \quad (2)$$

corresponding to yield-like quantities  $N_i$  and flow-like coefficients  $v_{2,i}$  evaluated in three representative centrality bins.

The model  $m(\theta)$  encodes a simple mapping between parameters and observables. The dominant dependence is captured by sector-wide amplitudes, with the yield-like observables  $N_i$  primarily controlled by the combination  $\kappa_N S$  and the flow-like observables  $v_{2,i}$  by  $\kappa_v \varepsilon_2$ . Weak cross-sensitivity between the two sectors is introduced through small mixing terms, ensuring that each observable group retains a subleading dependence on the parameters associated with the other sector. This structure is motivated by realistic heavy-ion simulations [36], where particle yields are largely governed by the overall entropy scale [37–39], while anisotropic flow reflects the response to the initial-state eccentricity [40, 41].

The centrality dependence is encoded through reference values  $N_i^{\text{ref}}$  and  $v_{2,i}^{\text{ref}}$ , which are guided by representative experimental measurements in different centrality classes [42, 43] and serve to anchor the model to realistic observable scales, reflecting the variation of entropy and eccentricity across these bins. The model predictions are constructed by rescaling these reference values through parameter-dependent amplitudes, supplemented by mild bin-to-bin modulations so that different centrality bins probe slightly different directions in parameter space.

An important advantage of this setup is that the forward model is analytic and inexpensive to evaluate, allowing posterior distributions to be computed directly without the need for surrogate models or emulators [18, 44]. This avoids additional sources of approximation and uncertainty that are unrelated to the statistical questions addressed here, and ensures that any differences observed between inference strategies can be unambiguously attributed to their statistical treatment, rather than to model approximations. We adopt broad uniform priors over all parameters, so that the posterior is primarily driven by the likelihood.

Pseudo-data are generated from a fixed reference parameter

point  $\theta_*$  by adding Gaussian fluctuations,

$$d = m(\theta_*) + \delta, \quad \delta \sim \mathcal{N}(0, \Sigma), \quad (3)$$

where  $m(\theta)$  denotes the model prediction and  $\Sigma$  is the covariance matrix. The covariance is written in block form as

$$\Sigma = \begin{pmatrix} \Sigma_1 & \Sigma_{12} \\ \Sigma_{21} & \Sigma_2 \end{pmatrix}, \quad (4)$$

where  $\Sigma_1$  and  $\Sigma_2$  describe correlations within the yield and flow sectors, and  $\Sigma_{12}$  encodes correlations between them. Within each sector, centrality bins are correlated over a finite range, introducing nontrivial bin-to-bin correlations while preserving partial independence.

Cross-dataset correlations are introduced through the off-diagonal block  $\Sigma_{12} = \rho \tilde{\Sigma}_{12}$  [35], where  $\tilde{\Sigma}_{12}$  defines a fixed correlation pattern and the parameter  $\rho$  controls the overall strength of correlations between the two observable groups.<sup>1</sup> The resulting correlation matrices are illustrated in Fig. 1. The limit  $\rho = 0$  corresponds to statistically independent datasets, while  $\rho \sim \mathcal{O}(0.1-1)$  spans weak to strong correlations. By varying  $\rho$ , we continuously interpolate between these regimes, allowing us to systematically probe the impact of cross-dataset correlations on Bayesian inference. In the following,  $\rho$  serves as the primary control parameter of the study.

### 3. Sequential Bayesian inference framework

With this setup in place, we now turn to the statistical framework used to combine the datasets and extract parameter constraints. We consider the problem of inferring model parameters  $\theta$  from two datasets, denoted  $D_1$  and  $D_2$ . In the present study, these correspond to the two observable groups introduced in Section 2, namely yield-like observables  $D_1 = \{N_i\}$  and flow-like observables  $D_2 = \{v_{2,i}\}$ , although the discussion below is general and does not depend on their specific physical interpretation. The model prediction for the full dataset is written as  $m(\theta)$ , and the measured data vector is denoted by  $d$ . The joint posterior distribution is given by Bayes' theorem [16, 17],

$$p(\theta|D_1, D_2) \propto p(D_1, D_2|\theta) p(\theta), \quad (5)$$

where  $p(\theta)$  is the prior and  $p(D_1, D_2|\theta)$  is the likelihood for the combined dataset. This expression defines the reference result against which all other inference procedures will be compared.

Using the chain rule of probability, the joint likelihood can be written exactly as  $p(D_1, D_2|\theta) = p(D_2|D_1, \theta) p(D_1|\theta)$ , which leads to the sequential form of the posterior,

$$p(\theta|D_1, D_2) \propto p(D_2|D_1, \theta) p(\theta|D_1), \quad (6)$$

where  $p(\theta|D_1) \propto p(D_1|\theta) p(\theta)$  denotes the posterior obtained from the first dataset alone. This relation shows that sequential

Bayesian updating is, in principle, always well-defined: once the posterior  $p(\theta|D_1)$  is obtained, the second update is governed by the conditional likelihood  $p(D_2|D_1, \theta)$ . The question is therefore not whether sequential inference is valid, but how this conditional dependence is treated in practice.

A commonly used approximation is to replace the conditional likelihood by the marginal likelihood  $p(D_2|\theta)$ , leading to a factorized sequential update,

$$p_{\text{fact}}(\theta|D_1, D_2) \propto p(D_2|\theta) p(\theta|D_1). \quad (7)$$

This form is widely adopted in multi-stage Bayesian analyses, where posterior distributions from earlier datasets are used as effective priors for subsequent updates. Under the assumption that the datasets are conditionally independent,  $p(D_2|D_1, \theta) = p(D_2|\theta)$ , the factorized update reproduces the joint posterior exactly.

When the datasets are correlated, the assumption of conditional independence is violated, and the conditional and marginal likelihoods differ,  $p(D_2|D_1, \theta) \neq p(D_2|\theta)$ . In this case, the factorized update no longer reproduces the result of a joint analysis. The discrepancy arises because the second dataset generally contains both independent and correlated components relative to  $D_1$ . The conditional likelihood  $p(D_2|D_1, \theta)$  isolates only the information in  $D_2$  that is not already encoded in  $D_1$ , whereas the marginal likelihood  $p(D_2|\theta)$  treats all fluctuations as independent. As a result, the factorized update effectively reuses information shared between the datasets, counting correlated contributions more than once.<sup>2</sup> In this sense, the factorized sequential update corresponds to an inference in which cross-dataset correlations are neglected. The resulting discrepancy therefore reflects a more general consequence of ignoring correlations in the likelihood, independent of whether the analysis is performed sequentially or jointly.

These considerations can be made explicit for Gaussian likelihoods. We consider a Gaussian likelihood for the full data vector  $d = (d_1, d_2)$ ,

$$\log \mathcal{L}_{\text{joint}}(\theta) = -\frac{1}{2}(d - m(\theta))^T \Sigma^{-1} (d - m(\theta)) - \frac{1}{2} \log \det \Sigma + \text{const}, \quad (8)$$

where  $\Sigma$  is the covariance matrix (4) defined in Section 2. The conditional structure of the likelihood can be made explicit by reorganizing the quadratic form in Eq. (8), separating contributions associated with  $d_1$  and  $d_2$ . This decomposition, derived explicitly in Appendix B, leads to a factorized representation in which the second term corresponds to the conditional likelihood  $p(D_2|D_1, \theta)$ .

For a Gaussian likelihood, the conditional distribution  $p(D_2|D_1, \theta)$  takes a Gaussian form, with covariance given by

<sup>1</sup>Even for  $\rho = 1$ , the presence of independent fluctuations within each dataset prevents perfect correlation between  $D_1$  and  $D_2$ . As a result, the datasets remain only partially correlated, with a finite conditional covariance.

<sup>2</sup>This behavior is closely related to what is often called ‘‘double counting’’ or ‘‘double-dipping’’ in Bayesian analysis. More commonly, these terms refer to reusing the same data both to construct a prior and to compute a likelihood [20]. In the present context, the issue arises instead from correlations between datasets: if these correlations are ignored, the factorized update treats shared fluctuations in  $D_1$  and  $D_2$  as independent evidence, effectively counting the same underlying information multiple times.

the Schur complement,

$$\Sigma_{2|1} = \Sigma_2 - \Sigma_{21}\Sigma_1^{-1}\Sigma_{12}, \quad (9)$$

and mean

$$\mu_{2|1}(\theta) = m_2(\theta) + \Sigma_{21}\Sigma_1^{-1}(d_1 - m_1(\theta)), \quad (10)$$

where  $m_1(\theta)$  and  $m_2(\theta)$  denote the model predictions restricted to the two datasets.<sup>3</sup> These expressions follow directly from the block structure of the covariance matrix and its inverse, as detailed in [Appendix B](#). The corresponding conditional log-likelihood  $\log p(D_2|D_1, \theta)$  is

$$\log \mathcal{L}_{2|1}(\theta) = -\frac{1}{2}(d_2 - \mu_{2|1}(\theta))^T \Sigma_{2|1}^{-1}(d_2 - \mu_{2|1}(\theta)) - \frac{1}{2} \log \det \Sigma_{2|1} + \text{const} \quad (11)$$

The conditional mean (10) removes the component of  $d_2$  that can be inferred from  $d_1$ , while the Schur-complement covariance (9) accounts for the corresponding reduction in uncertainty. Together, these terms ensure that the update incorporates only the component of  $D_2$  that is independent of  $D_1$ , thereby recovering the joint likelihood.

This behavior becomes particularly transparent in the limiting case of perfectly correlated datasets. When  $D_2$  is fully determined by  $D_1$ , the conditional mean becomes fully determined by  $d_1$  and the Schur-complement covariance vanishes, so that the conditional likelihood becomes independent of  $\theta$ . As a result, the second update introduces no additional constraint. In contrast, the factorized update continues to treat  $D_2$  as independent, artificially tightening the posterior by reusing the same underlying fluctuations. This provides a direct illustration of how neglecting correlations leads to an overcounting of information. The limiting case therefore serves as a simple consistency check: only information in  $D_2$  that is not already implied by  $D_1$  should contribute to the sequential update.

## 4. Results and discussion

We examine how correlations between datasets affect sequential Bayesian inference within the controlled setup introduced above. To this end, we compare three inference strategies: joint inference using the full likelihood [Eq. (5)], sequential updating with a factorized likelihood [Eq. (7)], and sequential updating using the conditional likelihood  $p(D_2|D_1, \theta)$  [Eq. (6)]. This comparison isolates the role of cross-dataset correlations and provides a direct test of how different implementations of sequential inference impact the resulting posterior. The results are organized to progressively connect: (i) the structure of parameter constraints (Section 4.1), (ii) the decomposition of information between datasets (Section 4.2), (iii) the

<sup>3</sup>The expressions above coincide with the standard conditioning formulas of a multivariate Gaussian distribution. In Gaussian process regression and emulator construction, the same relations define predictive means and covariances conditioned on training data [44], with the training set playing a role analogous to  $D_1$ .

resulting posterior distortions (Section 4.3), (iv) their quantitative impact (Section 4.4), and (v) the broader interpretation and implications of these effects (Section 4.5).

In the Gaussian approximation, parameter constraints are conveniently characterized by the Fisher information matrix, defined through the local quadratic expansion of the log-likelihood,  $\log \mathcal{L}(\theta) \simeq -\frac{1}{2} \delta\theta^T F \delta\theta + \dots$ . In terms of the model Jacobian  $J = \partial m / \partial \theta$  and covariance matrix, this can be written as  $F = J^T \Sigma^{-1} J$ . As shown in [Appendix B](#), this structure follows directly from the quadratic form of the Gaussian likelihood and makes explicit how cross-dataset correlations enter parameter inference through couplings between different observables. In the following, we use the Fisher matrix as a local measure of information to analyze how correlations modify the contribution of different datasets.

### 4.1. Sensitivity structure and parameter constraints

Before presenting the results, it is useful to clarify the role of correlations in the present setup by distinguishing between two conceptually different sources. First, correlations may arise from the shared dependence of observables on common model parameters, which determines how different datasets constrain overlapping directions in parameter space. Second, correlations may arise from statistical dependence between the datasets themselves, as encoded in the covariance matrix. In the following, we will explicitly refer to the latter as cross-dataset correlations. It is these cross-dataset correlations that lead to the breakdown of likelihood factorization.

To make this distinction concrete, we examine how the two datasets constrain the model parameters at the level of local sensitivities. This identifies the parameter directions along which different datasets exhibit overlapping constraints, which in turn determine where correlations can have the largest impact. To this end, we introduce a weighted sensitivity matrix

$$\tilde{J}_{\alpha i} = \frac{1}{\sigma_\alpha} \frac{\partial m_\alpha}{\partial \theta_i}, \quad (12)$$

which measures the local response of each observable in units of its statistical uncertainty. The sensitivity matrix also provides a direct link to the information content of the likelihood in parameter space. In terms of the Fisher information matrix  $F = J^T \Sigma^{-1} J$ , for uncorrelated observables, where the covariance is diagonal,  $\Sigma_{\alpha\beta} = \sigma_\alpha^2 \delta_{\alpha\beta}$ , this reduces to  $F_{ij} = \sum_\alpha \tilde{J}_{\alpha i} \tilde{J}_{\alpha j}$ . In this sense, the weighted sensitivities provide a simple proxy for how different observables contribute to parameter constraints.

For each dataset  $g \in \{D_1, D_2\}$ , we define an aggregated sensitivity strength

$$S_i^{(g)} = \left[ \sum_{\alpha \in g} \tilde{J}_{\alpha i}^2 \right]^{1/2}, \quad (13)$$

which provides a compact measure of how strongly parameter  $\theta_i$  is constrained by dataset  $g$ . The resulting sensitivity structure, shown in [Fig. 2](#), exhibits a clear hierarchy. The yield-like observables primarily constrain  $S$  and  $\kappa_N$ , while the flow-like observables primarily constrain  $\varepsilon_2$  and  $\kappa_v$ . In addition, the cross-sector sensitivity is asymmetric: the flow observables retain a

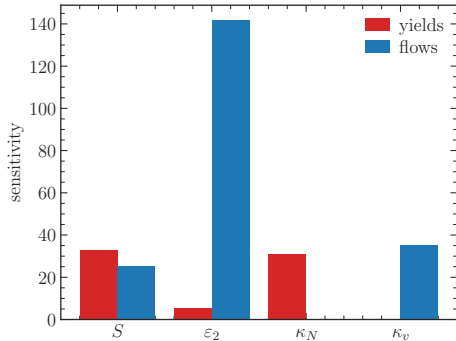


Figure 2: Aggregated sensitivity strength of the yield-like ( $D_1$ ) and flow-like ( $D_2$ ) observable groups to each model parameter, evaluated at the reference point  $\theta_*$ .

non-negligible dependence on  $S$ , whereas the yield observables are only weakly sensitive to  $\varepsilon_2$ . This asymmetry follows directly from the model construction<sup>4</sup> and provides a minimal realization of partially overlapping constraints.

#### 4.2. Information decomposition and cross-dataset redundancy

These sensitivity patterns identify the parameter directions along which the two datasets probe overlapping sensitivities, and therefore where cross-dataset correlations can influence parameter inference. We now quantify this effect by examining how the covariance structure modifies the information content of the likelihood. As shown in Appendix B, this modification can be understood in terms of the conditional decomposition of the likelihood, which induces a corresponding decomposition of Fisher information.

We focus on the contribution of the second dataset  $D_2$ . When correlations are ignored, its contribution to parameter constraints is described by the Fisher matrix

$$F_2 = J_2^T \Sigma_2^{-1} J_2, \quad (14)$$

where  $J_2 = \partial m_2 / \partial \theta$  is the Jacobian of the model prediction for  $D_2$ . This matrix represents the information that  $D_2$  appears to provide when treated as statistically independent from  $D_1$ .

When the datasets are correlated, part of the information attributed to  $D_2$  is already encoded in  $D_1$ . The relevant quantity for sequential inference is therefore the conditional contribution obtained from  $p(D_2|D_1, \theta)$ , which isolates the component of  $D_2$  that is independent of  $D_1$ . For a Gaussian likelihood, this distribution has covariance  $\Sigma_{2|1}$  given by the Schur complement [Eq. (9)] and mean  $\mu_{2|1}(\theta)$  [Eq. (10)]. The corresponding Jacobian follows from differentiating the conditional mean,

$$J_{2|1} = \frac{\partial \mu_{2|1}(\theta)}{\partial \theta} = J_2 - \Sigma_{21} \Sigma_1^{-1} J_1, \quad (15)$$

<sup>4</sup>In realistic heavy-ion dynamics [36], a larger entropy scale  $S$  generally leads to a longer system lifetime and enhanced development of anisotropic flow, resulting in larger  $v_2$ . In contrast, variations in the initial eccentricity  $\varepsilon_2$  have only a weak impact on integrated yields. This motivates the asymmetric cross-sector sensitivity in the reduced model.

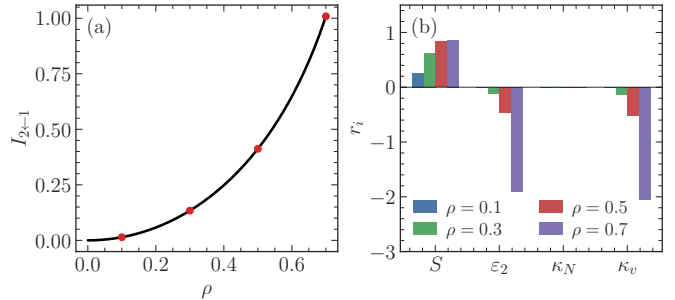


Figure 3: (a) Data-space information flow  $I_{2|1}$  as a function of the correlation strength  $\rho$ . (b) Corresponding parameter-resolved redundancy measure  $r_i$  for selected values of  $\rho$ .

as derived explicitly in Appendix B, showing that the response of  $D_2$  is reduced by the component that can be predicted from  $D_1$ . The conditional Fisher matrix then becomes

$$F_{2|1} = J_{2|1}^T \Sigma_{2|1}^{-1} J_{2|1}, \quad (16)$$

which quantifies the genuinely new information provided by  $D_2$ . As shown in Appendix B, cross-dataset correlations modify the joint Fisher matrix through the block structure of the covariance, leading to a decomposition in which the total information can be written as the sum of the contribution from  $D_1$  and the conditional contribution from  $D_2$ .

This separation can also be understood directly at the level of the data, where it is expressed in terms of the covariance matrices. The conditional covariance  $\Sigma_{2|1}$  represents the uncertainty in  $D_2$  that remains after accounting for correlations with  $D_1$ , while the difference between  $\Sigma_2$  and  $\Sigma_{2|1}$  encodes the component of  $D_2$  that is predictable from  $D_1$ . A convenient scalar measure of this effect, which we refer to as the information flow from  $D_1$  to  $D_2$ , is given by

$$I_{2|1} = \frac{1}{2} \log \frac{\det \Sigma_2}{\det \Sigma_{2|1}}, \quad (17)$$

which quantifies the reduction in uncertainty volume of  $D_2$  due to knowledge of  $D_1$ . In this sense,  $I_{2|1}$  measures how much of the variation in  $D_2$  can be inferred from  $D_1$  through correlations.

This reduction in data-space uncertainty translates into a corresponding modification of information in parameter space. The difference between the marginal and conditional Fisher matrices,  $\Delta F_{2|1} = F_2 - F_{2|1}$ , therefore quantifies the information in  $D_2$  that is not independent of  $D_1$ . To characterize this effect at the level of individual parameters, we introduce a redundancy measure

$$r_i = 1 - \frac{(F_{2|1})_{ii}}{(F_2)_{ii}}, \quad (18)$$

which represents the fraction of the marginal information in parameter  $\theta_i$  that is modified by conditioning.<sup>5</sup>

<sup>5</sup>This definition is based on the diagonal elements of the Fisher matrix and therefore depends on the chosen parameter basis. In general, the Fisher ma-

The behavior of these quantities is illustrated in Fig. 3. Figure 3(a) shows that the information flow  $I_{2 \leftarrow 1}$  increases with the correlation strength  $\rho$ , indicating that a growing fraction of the fluctuations in  $D_2$  becomes predictable from  $D_1$ . This reduction in data-space uncertainty propagates into parameter space in a non-uniform way. Figure 3(b) shows that the resulting redundancy varies strongly across parameters. This pattern can be understood in connection with the sensitivity structure shown in Fig. 2. Parameters such as  $\varepsilon_2$  and  $\kappa_v$ , which are primarily constrained by the flow observables ( $D_2$ ) but remain indirectly coupled to  $D_1$  through shared dependencies (notably via  $S$ ), exhibit the largest deviations. In contrast, parameters such as  $\kappa_N$ , to which  $D_2$  is only weakly sensitive, remain largely unaffected, while parameters like  $S$ , which are constrained by both datasets, show more moderate behavior.

In some directions, notably along  $\varepsilon_2$  and  $\kappa_v$ , the redundancy measure becomes negative, indicating that correlations can reshape the geometry of parameter constraints, enhancing curvature along certain directions rather than simply removing information. The dependence on  $\rho$  is also strongly parameter-dependent:  $S$  exhibits a gradual increase in redundancy, while  $\varepsilon_2$  and  $\kappa_v$  show a rapid decrease to large negative values, reflecting a correlation-induced reshaping of the constraint geometry.

Together, these results show that cross-dataset correlations induce a decomposition of information, separating the contribution of  $D_2$  into components that are genuinely new and components that are redundant with  $D_1$ . This decomposition provides a direct link between data-level correlations and their parameter-dependent impact on inference. In the following, we use this framework to analyze how these effects propagate into posterior distributions.

#### 4.3. Impact on posterior inference

Having established how correlations modify the information carried by  $D_2$ , we now examine how these effects appear in the posterior distribution. As discussed in Section 3, factorized sequential updating reproduces the joint posterior only in the limit of conditional independence, so deviations from the joint result provide a direct measure of the impact of correlations.

The effect is illustrated in Fig. 4. For  $\rho = 0$ , all inference methods coincide (not shown), consistent with the factorization of the likelihood. As  $\rho$  increases, systematic deviations develop between the factorized sequential result and the joint posterior, while the conditional sequential result remains consistent with the joint inference. The magnitude of these deviations grows continuously with  $\rho$ .

We have also verified that sequential updating based on the conditional likelihood yields results that are independent of the order in which the datasets are incorporated, in agreement with the joint posterior (not shown). In contrast, factorized sequential updates are likewise order-independent, since they correspond to a product of marginal likelihood terms, but generally

---

trix is not diagonal, and parameter constraints are determined by its full eigenstructure. As a result, individual parameters do not correspond uniquely to independent directions in parameter space, and correlations may act on linear combinations of parameters rather than on individual components.

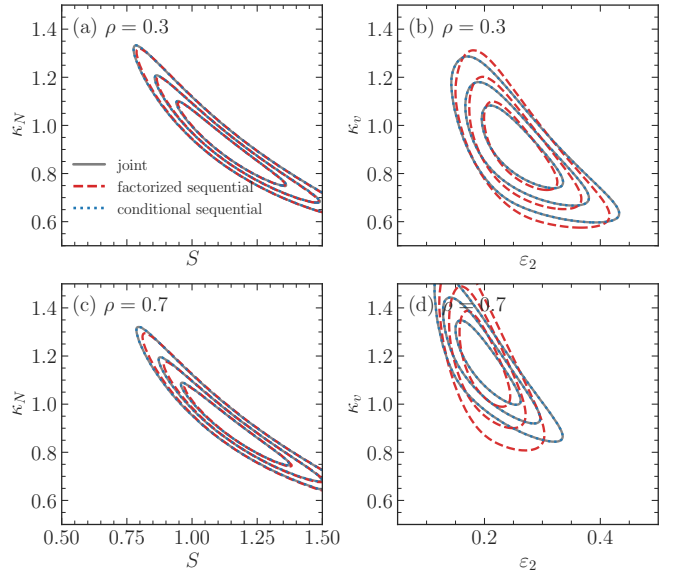


Figure 4: Posterior contours for joint inference (black solid), factorized sequential updating (red dashed), and conditional sequential updating (blue dotted), shown at  $\rho = 0.3$  (top) and  $\rho = 0.7$  (bottom). Left panels correspond to the  $(S, \kappa_N)$  plane, and right panels to the  $(\varepsilon_2, \kappa_v)$  plane.

do not reproduce the joint result once cross-dataset correlations are present.

The structure of these deviations can be understood in terms of the information decomposition introduced in Section 4.2. The factorized sequential update neglects the distinction between marginal and conditional information, leading to distortions along directions where this difference is largest. This is reflected in Fig. 4, where the deviations are most pronounced in the  $(\varepsilon_2, \kappa_v)$  plane, while remaining comparatively mild in the  $(S, \kappa_N)$  plane. This pattern reflects how correlations modify the effective information associated with different parameter directions: directions strongly affected by correlations exhibit the largest distortions, while those for which the marginal and conditional structures remain similar are comparatively stable.

More generally, the posterior distortions reflect not only a removal of redundant information, but a restructuring of parameter constraints induced by correlations. As a result, the effect is anisotropic, with both suppression and enhancement of constraints along different parameter directions, rather than a uniform overcounting of information.

#### 4.4. Quantifying deviations from joint inference

Having established the qualitative behavior, we now quantify the deviation between sequential inference and the joint result using the Kullback–Leibler (KL) divergence [45] between a sequential posterior  $p_{\text{seq}}(\theta)$  and the joint posterior  $p_{\text{joint}}(\theta)$ ,

$$D_{\text{KL}}(p_{\text{seq}} \| p_{\text{joint}}) = \int d\theta p_{\text{seq}}(\theta) \log \frac{p_{\text{seq}}(\theta)}{p_{\text{joint}}(\theta)}. \quad (19)$$

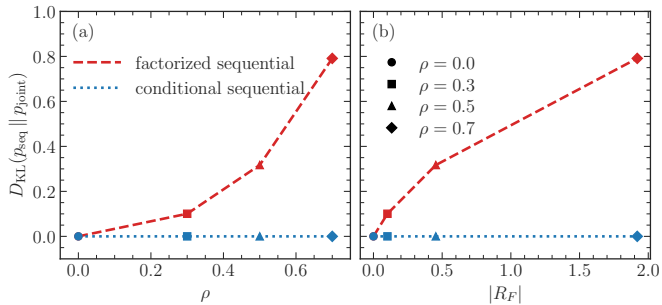


Figure 5: (a) Kullback–Leibler (KL) divergence between sequential posteriors and the joint posterior as a function of the correlation strength  $\rho$ , for factorized (red) and conditional (blue) sequential updating. (b) KL divergence as a function of the normalized Fisher-level redundancy  $R_F$ .

This quantity measures the information loss incurred when the joint posterior is approximated by a sequential construction.<sup>6</sup>

The results are shown in Fig. 5. Panel (a) displays the KL divergence as a function of the correlation strength  $\rho$ . For  $\rho = 0$ , the divergence vanishes for both sequential methods, reflecting the factorization of the likelihood in the absence of cross-dataset correlations. As  $\rho$  increases, the factorized sequential result departs monotonically from the joint posterior, while the conditional sequential result remains consistent with it over the full range of  $\rho$ . The smooth growth of the divergence indicates that the effect of cross-dataset correlations accumulates continuously, rather than appearing as a threshold phenomenon.

Panel (b) relates the KL divergence directly to the redundancy structure introduced in Section 4.2. Specifically, we consider the normalized Fisher-level redundancy

$$R_F = \frac{\text{Tr}(F_2 - F_{2|1})}{\text{Tr}(F_2)}, \quad (20)$$

which measures the fraction of the apparent information in  $D_2$  that is not independent of  $D_1$ . Since  $R_F$  depends only on the model and covariance structure, it is the same for both sequential inference methods. The figure shows a clear monotonic relation between  $D_{\text{KL}}$  and  $R_F$  for the factorized sequential update, demonstrating that the deviation from the joint posterior is controlled by the mismatch between marginal and conditional information. In contrast, the conditional sequential update remains consistent with the joint posterior for all values of  $R_F$ , yielding vanishing KL divergence. This comparison makes explicit that redundancy alone does not induce errors; rather, deviations arise when this redundancy is not properly accounted for in the inference procedure.

The KL divergence provides a complementary perspective to the parameter-level analysis presented in Section 4.3. While Fig. 4 illustrates posterior deviations in selected parameter subspaces, the KL divergence captures the cumulative effect of

<sup>6</sup>KL divergence is commonly used in Bayesian analyses to quantify the information gain from prior to posterior distributions. In heavy-ion physics, it has been used, for example, to assess the constraining power of different observables by the JETSCAPE Collaboration [9, 10, 46]. More generally, it provides a measure of the change in statistical uncertainty induced by new data.

these deviations across the full parameter space. It therefore confirms that the discrepancies observed in specific parameter pairs reflect a global restructuring of the posterior, rather than isolated effects restricted to particular projections.

#### 4.5. Interpretation and implications

These results provide a unified interpretation of the mechanisms identified across the previous subsections. Cross-dataset correlations reorganize the information carried by different observables, modifying how constraints are distributed across parameter space. The resulting deviations from joint inference therefore reflect a structured mismatch between the marginal and conditional organization of the likelihood, rather than a uniform overcounting of information.

These results isolate a fundamental source of discrepancy in multi-stage Bayesian inference: the structure of the likelihood itself. Even in a Gaussian setting without multi-modality [21], factorized updates fail once cross-dataset correlations are present, demonstrating that consistent treatment of covariance is a necessary condition for reliable sequential inference. More broadly, the analysis shows that the error of factorized sequential inference is not merely a consequence of the presence of correlations, but is quantitatively controlled by how those correlations redistribute information between datasets. Since the factorized sequential update corresponds to an inference in which cross-dataset correlations are neglected, the same type of bias arises in any analysis that ignores such correlations at the likelihood level.

## 5. Summary and conclusions

In this work, we have investigated sequential Bayesian inference in the presence of correlated datasets within a controlled framework. While Bayesian updating can always be formulated sequentially through the conditional likelihood, practical implementations often rely on a factorized update that assumes conditional independence. We have shown that this approximation is valid only in the absence of correlations, and otherwise leads to systematic deviations from the joint posterior.

Using a reduced model with a tunable covariance structure, we find that factorized sequential updates depart increasingly from the joint result as the strength of cross-dataset correlations grows, while conditional updating remains fully consistent with the joint posterior. These deviations can be understood in terms of an information decomposition, in which correlations partition the contribution of a dataset into components that are genuinely new and components that are not independent of previously incorporated data. This decomposition is strongly parameter-dependent, reflecting the interplay between covariance structure and parameter sensitivities, and provides a quantitative link between dataset correlations and inference error.

More generally, factorized sequential updating corresponds to performing a joint inference under an implicit assumption of statistical independence. When this assumption is violated, shared information is effectively overcounted, leading

to systematically distorted and overconstrained posterior estimates. Consistent sequential inference therefore requires a proper treatment of correlations at the likelihood level within a common probabilistic framework.

These considerations extend beyond explicitly sequential workflows. In many analyses, priors encode information from previous datasets and implicitly assume statistical independence from the data incorporated at later stages. The framework developed here provides a way to assess the validity of this assumption and to quantify its impact.

Although demonstrated in a reduced setting, the conclusions are broadly applicable to multi-dataset Bayesian analyses. They provide both a conceptual framework and a practical diagnostic: deviations from joint inference are controlled by how correlations redistribute information across parameter space, as determined by the interplay between dataset covariance and parameter sensitivities.

## Acknowledgements

The author acknowledges valuable discussions with S. Jaiswal, P. M. Jacobs, and other members of the JETSCAPE Collaboration. This work was supported in part by the U.S. Department of Energy, Office of Science, Office of Nuclear Physics under Grant No. DE-AC02-05CH11231. The author acknowledges the use of ChatGPT for assistance with grammar refinement and clarity improvement during manuscript preparation.

## Appendix A. Model construction and implementation

In this appendix, we provide the explicit construction of the reduced model used in the main text. The purpose of this model is not to reproduce realistic heavy-ion data, but to provide a controlled and transparent setting in which different classes of observables probe partially overlapping aspects of a small set of parameters. The guiding principle is to retain the minimal structure necessary to capture multi-observable inference, while keeping the model simple enough to allow direct evaluation of the likelihood without introducing additional complications such as emulators or surrogate models.

The model depends on four parameters,  $\theta = (S, \varepsilon_2, \kappa_N, \kappa_v)$ . Here  $S$  represents an overall initial scale (entropy-like quantity), and  $\varepsilon_2$  an eccentricity-like parameter controlling initial anisotropy. The parameters  $\kappa_N$  and  $\kappa_v$  describe how efficiently these quantities are converted into yield-like and flow-like observables, respectively. In this way,  $(S, \kappa_N)$  primarily control yields, while  $(\varepsilon_2, \kappa_v)$  primarily control flow, although this separation is only approximate (see below).

We consider two groups of observables evaluated in three centrality bins  $i = 1, 2, 3$ , corresponding to representative central (0–10%), mid-central (20–30%), and peripheral (40–50%) collisions. The first group consists of yield-like observables  $N_i$ , and the second of elliptic flow coefficients  $v_{2,i}$ , forming the data vector  $d = (N_1, N_2, N_3, v_{2,1}, v_{2,2}, v_{2,3})$ . To set realistic overall scales, we anchor the observables to fixed reference values

inspired by heavy-ion measurements [42, 43], using  $N^{\text{ref}} = (1447.5, 649.0, 261.0)$  and  $v_2^{\text{ref}} = (0.0359, 0.0831, 0.0994)$ . These reference values encode the dominant centrality dependence of the system, effectively capturing the variation of entropy and eccentricity across centrality classes. All observables are normalized at a reference parameter point  $\theta_\star = (S, \varepsilon_2, \kappa_N, \kappa_v)_\star = (1.0, 0.25, 1.0, 1.0)$ , so that the model reproduces the reference values at this point.

The observables are constructed multiplicatively as

$$N_i(\theta) = N_i^{\text{ref}} \left( \frac{A_N(\theta)}{A_N(\theta_\star)} \right) Y_i(\theta), \quad v_{2,i}(\theta) = v_{2,i}^{\text{ref}} \left( \frac{A_v(\theta)}{A_v(\theta_\star)} \right) V_i(\theta), \quad (\text{A.1})$$

which separates the dominant parameter dependence from sub-leading bin-dependent effects. The dominant structure is encoded in sector-wide amplitudes  $A_N(\theta) = \kappa_N S + \alpha_N \varepsilon_2$  and  $A_v(\theta) = \kappa_v \varepsilon_2 + \alpha_v S$ , with  $\alpha_N = 0.12$  and  $\alpha_v = 0.18$ . These cross-coupling terms are introduced to mimic the fact that, in realistic simulations, different observables are not fully independent but instead probe overlapping aspects of the underlying dynamics. The choice  $\alpha_v > \alpha_N$  ensures that the flow observables retain a stronger sensitivity to the yield-side parameter  $S$  than vice versa, producing the asymmetric coupling structure discussed in the main text (see Fig. 2).

To break exact factorization within each observable group, we introduce mild centrality-dependent shape factors. For the yields,  $Y_i(\theta) = 1 + a_i^{(S)}(S - S_\star) + a_i^{(\kappa_N)}(\kappa_N - \kappa_{N,\star})$ , and for the flow observables,  $V_i(\theta) = 1 + b_i^{(\varepsilon_2)}(\varepsilon_2 - \varepsilon_{2,\star}) + b_i^{(\kappa_v)}(\kappa_v - \kappa_{v,\star})$ . The coefficients,  $a_i$  and  $b_i$ , are chosen to be small, so that these terms act as perturbations around the dominant amplitude dependence. Their role is to introduce mild bin-to-bin variations and to avoid exact degeneracies, without obscuring the main parameter structure.

Pseudo-data are generated from the reference point as  $d = m(\theta_\star) + \delta$ , with Gaussian fluctuations  $\delta \sim \mathcal{N}(0, \Sigma)$ . The covariance matrix is constructed in block form to separate correlations within and between the two observable groups. Within each observable group, bin-to-bin correlations are modeled using a short-range kernel [12, 13]. For centrality bins  $i, j = 1, 2, 3$ , we define a correlation matrix  $C_{ij} = \exp(-|i - j|/\ell)$  with correlation length  $\ell = 1.0$ , so that neighboring bins are more strongly correlated than distant ones. To retain a finite level of independent fluctuations, this correlated structure is combined with an uncorrelated component. The resulting intra-group covariance matrix for a given observable type  $X \in \{N, v_2\}$  is constructed as

$$\Sigma_X^{ij} = \sigma_{X,i} \sigma_{X,j} \left[ (1 - f_{\text{ind}}) C_{ij} + f_{\text{ind}} \delta_{ij} \right], \quad (\text{A.2})$$

where  $f_{\text{ind}} = 0.4$  controls the fraction of independent noise and  $\delta_{ij}$  is the Kronecker delta. This form ensures that correlations decay with bin separation while preserving nonzero diagonal dominance. The overall fluctuation scale is set by ALICE-inspired absolute uncertainties for the selected Pb–Pb 2.76 TeV reference bins, multiplied by a uniform rescaling factor of 1.7. For the yield-like and flow-like observables, this corresponds to  $\sigma_N^{\text{obs}} = 1.7 \sigma_N^{\text{ref}}$ , and  $\sigma_{v_2}^{\text{obs}} = 1.7 \sigma_{v_2}^{\text{ref}}$ , where  $\sigma^{\text{ref}}$  denotes the baseline experimental uncertainties. This choice provides

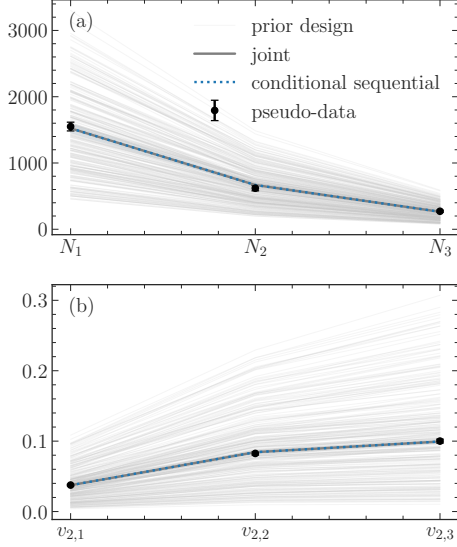


Figure A.6: Model predictions for yield-like (a) and flow-like (b) observables at  $\rho = 0.7$ . Gray lines denote prior design points, markers show pseudo-data, and curves correspond to joint and conditional sequential inference results.

a simplified heavy-ion-inspired noise model anchored to realistic observable scales, while avoiding a detailed reproduction of the full experimental covariance.

Cross-dataset correlations are introduced through the off-diagonal block  $\Sigma_{12}$  of the full covariance matrix (4). We construct it in factorized form as

$$\Sigma_{12}^{ij} = \rho \sigma_{N,i} \sigma_{v_2,j} C_{ij}, \quad (\text{A.3})$$

where the same short-range kernel  $C_{ij}$  is used to correlate nearby bins across the two observable groups. The parameter  $\rho$  controls the overall strength of cross-dataset correlations, with  $\rho = 0$  corresponding to statistically independent datasets and larger values introducing increasing levels of correlation. The full covariance matrix then takes the block form  $\Sigma = \begin{pmatrix} \Sigma_1 & \Sigma_{12} \\ \Sigma_{21} & \Sigma_2 \end{pmatrix}$ , with  $\Sigma_1 \equiv \Sigma_N$  and  $\Sigma_2 \equiv \Sigma_{v_2}$  (see Fig. 1).

Finally, we adopt a uniform prior over the parameter ranges  $S \in [0.5, 1.5]$ ,  $\varepsilon_2 \in [0.05, 0.5]$ ,  $\kappa_N \in [0.5, 1.5]$ , and  $\kappa_v \in [0.5, 1.5]$ . These ranges are chosen to be broad enough to encompass the relevant parameter space without imposing strong prior constraints. Parameter points leading to nonphysical (negative) observables are excluded by assigning them vanishing likelihood. Figure A.6 illustrates the resulting structure of the model and data. The prior design points span a broad region of observable space, while the posterior predictions from joint and conditional sequential inference collapse onto the pseudo-data. Here, the posterior predictions correspond to the posterior predictive mean, obtained by averaging model predictions over the full posterior distribution. This demonstrates that the model retains sufficient flexibility to describe the data while remaining simple enough to isolate the effects of correlations.

## Appendix B. Matrix structure of correlation effects

To clarify how correlations propagate from the data level to parameter inference, we examine the Gaussian likelihood in block form. The goal is to make explicit how the covariance structure modifies the information carried by different datasets, and how this modification is encoded in both the likelihood and its parameter-space representation.

We introduce residuals  $r_1 = d_1 - m_1(\theta)$  and  $r_2 = d_2 - m_2(\theta)$ , and write the covariance matrix as

$$\Sigma = \begin{pmatrix} \Sigma_1 & \Sigma_{12} \\ \Sigma_{21} & \Sigma_2 \end{pmatrix},$$

where  $\Sigma_{12}$  encodes cross-dataset correlations. The joint Gaussian likelihood can be written as

$$\mathcal{L}(\theta) = p(D_1, D_2 | \theta) \propto \exp \left[ -\frac{1}{2} Q_{\text{joint}} \right], \quad (\text{B.1})$$

with quadratic form

$$Q_{\text{joint}} = \begin{pmatrix} r_1 \\ r_2 \end{pmatrix}^T \Sigma^{-1} \begin{pmatrix} r_1 \\ r_2 \end{pmatrix}. \quad (\text{B.2})$$

The quadratic form measures the mismatch between data and model predictions, weighted by the inverse covariance. Correlations between datasets therefore enter through the off-diagonal blocks of  $\Sigma^{-1}$ , which couple the residuals  $r_1$  and  $r_2$ .

Using the block inverse of  $\Sigma$ , the quadratic form can be written as

$$Q_{\text{joint}} = r_1^T \Sigma_1^{-1} r_1 + (r_2 - \Sigma_{21} \Sigma_1^{-1} r_1)^T \Sigma_{2|1}^{-1} (r_2 - \Sigma_{21} \Sigma_1^{-1} r_1), \quad (\text{B.3})$$

where  $\Sigma_{2|1} = \Sigma_2 - \Sigma_{21} \Sigma_1^{-1} \Sigma_{12}$  is the Schur-complement covariance, representing the uncertainty in  $D_2$  that remains after accounting for correlations with  $D_1$ . This identity makes explicit that the joint likelihood factorizes exactly as  $p(D_1, D_2 | \theta) = p(D_1 | \theta) p(D_2 | D_1, \theta)$ . The second term can be written in terms of a conditional residual

$$r_{2|1} = r_2 - \Sigma_{21} \Sigma_1^{-1} r_1 = d_2 - \mu_{2|1}(\theta), \quad (\text{B.4})$$

where the conditional mean is given by

$$\mu_{2|1}(\theta) = m_2(\theta) + \Sigma_{21} \Sigma_1^{-1} (d_1 - m_1(\theta)). \quad (\text{B.5})$$

In this form, the second term describes fluctuations of  $D_2$  around the conditional mean  $\mu_{2|1}(\theta)$ , isolating the component that cannot be predicted from  $D_1$ .

To connect this structure to parameter inference, we expand the log-likelihood around a reference point  $\theta_*$ . Writing  $\delta\theta = \theta - \theta_*$ , the Gaussian likelihood takes the quadratic form

$$\log \mathcal{L}(\theta) \simeq -\frac{1}{2} \delta\theta^T F_{\text{joint}} \delta\theta + \text{const}, \quad (\text{B.6})$$

where the Fisher information matrix

$$F_{\text{joint}} = J^T \Sigma^{-1} J \quad (\text{B.7})$$

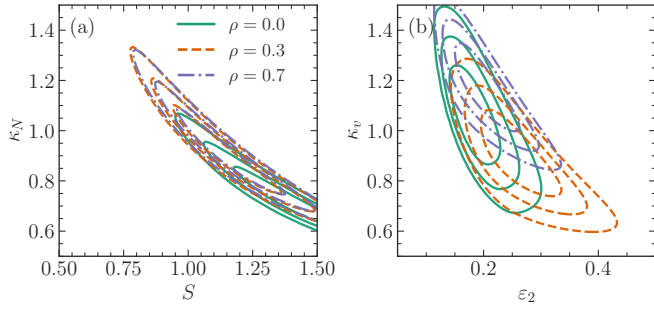


Figure B.7: Joint posterior distributions for three representative values of the cross-dataset correlation strength  $\rho$ . The left panel shows the  $(S, \kappa_N)$  plane and the right panel the  $(\epsilon_2, \kappa_v)$  plane. Contours correspond to  $\rho = 0.0$  (solid),  $\rho = 0.3$  (dashed), and  $\rho = 0.7$  (dash-dotted). All posteriors are obtained using the full joint likelihood.

is defined as the curvature of the joint log-likelihood, with  $J = \partial m / \partial \theta$  the model Jacobian. In this form, the Fisher matrix quantifies how sensitively the likelihood responds to variations in the model parameters. Comparing this expression with the quadratic form of the likelihood shows that each term of the form  $r^T \Sigma^{-1} r$  contributes a corresponding Fisher term  $J^T \Sigma^{-1} J$  in parameter space.

Differentiating the conditional mean yields the modified Jacobian

$$J_{2|1} = \frac{\partial \mu_{2|1}(\theta)}{\partial \theta} = J_2 - \Sigma_{21} \Sigma_1^{-1} J_1, \quad (\text{B.8})$$

where  $J_i = \partial m_i / \partial \theta$ . The corresponding Fisher contribution is

$$F_{2|1} = J_{2|1}^T \Sigma_{2|1}^{-1} J_{2|1}, \quad (\text{B.9})$$

while

$$F_1 = J_1^T \Sigma_1^{-1} J_1. \quad (\text{B.10})$$

The joint Fisher matrix can therefore be written as

$$F_{\text{joint}} = F_1 + F_{2|1}. \quad (\text{B.11})$$

This decomposition provides the parameter-space counterpart of the likelihood factorization above: the total information is the sum of the contribution from  $D_1$  and the independent component of  $D_2$ . In this representation, the effects of cross-dataset correlations do not appear as explicit cross terms, but are absorbed into the modified covariance  $\Sigma_{2|1}$  and response  $J_{2|1}$ .

From a complementary perspective, the same mechanism can be understood in terms of the shape of the likelihood over parameter space. Writing the inverse covariance in block form, the off-diagonal blocks of  $\Sigma^{-1}$  couple the residuals of the two datasets. Denoting this coupling by  $C$ , the quadratic form contains a cross term of the form  $-r_1^T C r_2$ , which encodes the effect of cross-dataset correlations. The posterior is therefore altered through a reshaping of the likelihood landscape, with the magnitude and direction of the effect determined by how the two datasets respond jointly to variations in  $\theta$ . Directions in which both residuals vary coherently are most strongly affected, while directions that primarily influence only one dataset remain comparatively insensitive.

This behavior is visible directly in Fig. B.7. As the correlation strength  $\rho$  increases, the posterior evolves continuously, reflecting a shift in the effective balance of constraints between the two observable groups. The effect is more pronounced in the  $(\epsilon_2, \kappa_v)$  plane than in the  $(S, \kappa_N)$  plane, consistent with the asymmetric sensitivity structure discussed in the main text. In this way, the off-diagonal structure of  $\Sigma^{-1}$  determines how correlations are projected into parameter space locally, while the induced reshaping of the likelihood governs how these effects accumulate to produce the global posterior distortions discussed in the main text.

## References

- [1] R. Trotta, Bayes in the sky: Bayesian inference and model selection in cosmology, *Contemp. Phys.* 49 (2008) 71–104. [arXiv:0803.4089](#), [doi:10.1080/00107510802066753](#).
- [2] D. MacKay, *Information Theory, Inference and Learning Algorithms*, Cambridge University Press, 2003. URL <https://books.google.com/books?id=AKuMj4PN EMC>
- [3] A. R. Liddle, Statistical methods for cosmological parameter selection and estimation, *Ann. Rev. Nucl. Part. Sci.* 59 (2009) 95–114. [arXiv:0903.4210](#), [doi:10.1146/annurev.nucl.010909.083706](#).
- [4] S. Pratt, E. Sangaline, P. Sorensen, H. Wang, Constraining the Eq. of State of Super-Hadronic Matter from Heavy-Ion Collisions, *Phys. Rev. Lett.* 114 (2015) 202301. [arXiv:1501.04042](#), [doi:10.1103/PhysRevLett.114.202301](#).
- [5] J. E. Bernhard, J. S. Moreland, S. A. Bass, J. Liu, U. Heinz, Applying Bayesian parameter estimation to relativistic heavy-ion collisions: simultaneous characterization of the initial state and quark-gluon plasma medium, *Phys. Rev. C* 94 (2) (2016) 024907. [arXiv:1605.03954](#), [doi:10.1103/PhysRevC.94.024907](#).
- [6] J. E. Bernhard, J. S. Moreland, S. A. Bass, Bayesian estimation of the specific shear and bulk viscosity of quark–gluon plasma, *Nature Phys.* 15 (11) (2019) 1113–1117. [doi:10.1038/s41567-019-0611-8](#).
- [7] G. Nijs, W. van der Schee, U. Gürsoy, R. Snellings, Transverse Momentum Differential Global Analysis of Heavy-Ion Collisions, *Phys. Rev. Lett.* 126 (20) (2021) 202301. [arXiv:2010.15130](#), [doi:10.1103/PhysRevLett.126.202301](#).
- [8] G. Nijs, W. van der Schee, U. Gürsoy, R. Snellings, Bayesian analysis of heavy ion collisions with the heavy ion computational framework Trajectum, *Phys. Rev. C* 103 (5) (2021) 054909. [arXiv:2010.15134](#), [doi:10.1103/PhysRevC.103.054909](#).
- [9] D. Everett, et al., Phenomenological constraints on the transport properties of QCD matter with data-driven model averaging, *Phys. Rev. Lett.* 126 (24) (2021) 242301. [arXiv:2010.03928](#), [doi:10.1103/PhysRevLett.126.242301](#).
- [10] D. Everett, et al., Multisystem Bayesian constraints on the transport coefficients of QCD matter, *Phys. Rev. C* 103 (5) (2021) 054904. [arXiv:2011.01430](#), [doi:10.1103/PhysRevC.103.054904](#).
- [11] W. Fan, et al., New metric improving Bayesian calibration of a multistage approach studying hadron and inclusive jet suppression, *Phys. Rev. C* 109 (6) (2024) 064903. [arXiv:2307.09641](#), [doi:10.1103/PhysRevC.109.064903](#).
- [12] S. Cao, et al., Determining the jet transport coefficient  $\hat{q}$  from inclusive hadron suppression measurements using Bayesian parameter estimation, *Phys. Rev. C* 104 (2) (2021) 024905. [arXiv:2102.11337](#), [doi:10.1103/PhysRevC.104.024905](#).
- [13] R. Ehlers, et al., Bayesian inference analysis of jet quenching using inclusive jet and hadron suppression measurements, *Phys. Rev. C* 111 (5) (2025) 054913. [arXiv:2408.08247](#), [doi:10.1103/PhysRevC.111.054913](#).
- [14] A. Mankolli, et al., Longitudinal Dynamics of Large and Small Systems from a 3D Bayesian Calibration of RHIC Top-energy Collision Data [arXiv:2601.17234](#).
- [15] L. Du, Multi-observable analysis of jet quenching using Bayesian inference with JETSCAPE, *Nucl. Phys. A* 1060 (2025) 123100. [doi:10.1016/j.nuclphysa.2025.123100](#).

- [16] D. S. Sivia, Data analysis : a Bayesian tutorial, second edition. Edition, Oxford science publications, Clarendon, Oxford, 2006.
- [17] U. von Toussaint, Bayesian inference in physics, Rev. Mod. Phys. 83 (2011) 943–999. doi:10.1103/RevModPhys.83.943.
- [18] J.-F. Paquet, Applications of emulation and Bayesian methods in heavy-ion physics, J. Phys. G 51 (10) (2024) 103001. arXiv:2310.17618, doi:10.1088/1361-6471/ad6a2b.
- [19] C. Bishop, Pattern Recognition and Machine Learning, Information Science and Statistics, Springer, 2006. URL <https://books.google.de/books?id=qWPwnQEACAAJ>
- [20] R. Van de Schoot, S. Depaoli, R. King, B. Kramer, K. Märtens, M. G. Tadesse, M. Vannucci, A. Gelman, D. Veen, J. Willemsen, et al., Bayesian statistics and modelling, Nature Reviews Methods Primers 1 (1) (2021) 1.
- [21] H. Roch, C. Shen, Learning informed prior distributions with normalizing flows for Bayesian analysis, Phys. Rev. C 113 (3) (2026) 034903. arXiv:2509.14911, doi:10.1103/PhysRevC.113.034903.
- [22] P. Bozek, Transverse-momentum–flow correlations in relativistic heavy-ion collisions, Phys. Rev. C 93 (4) (2016) 044908. arXiv:1601.04513, doi:10.1103/PhysRevC.93.044908.
- [23] M. Luzum, J.-Y. Ollitrault, Extracting the shear viscosity of the quark-gluon plasma from flow in ultra-central heavy-ion collisions, Nucl. Phys. A 904-905 (2013) 377c–380c. arXiv:1210.6010, doi:10.1016/j.nuclphysa.2013.02.028.
- [24] J.-Y. Ollitrault, Anisotropy as a signature of transverse collective flow, Phys. Rev. D 46 (1992) 229–245. doi:10.1103/PhysRevD.46.229.
- [25] L. Du, H. Gao, S. Jeon, C. Gale, Rapidity scan with multistage hydrodynamic and statistical thermal models, Phys. Rev. C 109 (1) (2024) 014907. arXiv:2302.13852, doi:10.1103/PhysRevC.109.014907.
- [26] D. Teaney, L. Yan, Triangularity and Dipole Asymmetry in Heavy Ion Collisions, Phys. Rev. C 83 (2011) 064904. arXiv:1010.1876, doi:10.1103/PhysRevC.83.064904.
- [27] L. Du, Kinematic and dynamical origins of mean-pT fluctuations in heavy-ion collisions, Phys. Lett. B 874 (2026) 140225. arXiv:2512.22715, doi:10.1016/j.physletb.2026.140225.
- [28] J. S. Moreland, J. E. Bernhard, S. A. Bass, Bayesian calibration of a hybrid nuclear collision model using p-Pb and Pb-Pb data at energies available at the CERN Large Hadron Collider, Phys. Rev. C 101 (2) (2020) 024911. arXiv:1808.02106, doi:10.1103/PhysRevC.101.024911.
- [29] L. Du, Advancing multimessenger approaches in heavy-ion collisions: Insights from electromagnetic probes, EPJ Web Conf. 339 (2025) 01016. arXiv:2503.09045, doi:10.1051/epjconf/202533901016.
- [30] A. Sorensen, et al., Dense nuclear matter equation of state from heavy-ion collisions, Prog. Part. Nucl. Phys. 134 (2024) 104080. arXiv:2301.13253, doi:10.1016/j.pnpnp.2023.104080.
- [31] L. Du, U. Heinz, Electromagnetic Tomography of Radial Flow in the Quark-Gluon Plasma, Phys. Rev. Lett. 136 (10) (2026) 102301. arXiv:2505.20752, doi:10.1103/PhysRevLett.136.102301.
- [32] M. Arslanok, et al., Hot QCD White Paper arXiv:2303.17254.
- [33] L. Du, A. Sorensen, M. Stephanov, The QCD phase diagram and Beam Energy Scan physics: A theory overview, Int. J. Mod. Phys. E 33 (07) (2024) 2430008. arXiv:2402.10183, doi:10.1142/9789811294679\_0007.
- [34] Y. Yamauchi, L. Buskirk, P. Giuliani, K. Godbey, Normalizing Flows for Bayesian Posteriors: Reproducibility and Deployment arXiv:2310.04635.
- [35] R. A. Soltz, D. A. Hangal, A. Angerami, Simple model to investigate jet quenching and correlated errors for centrality-dependent nuclear modification factors in relativistic heavy-ion collisions, Phys. Rev. C 111 (3) (2025) 034911. arXiv:2412.03724, doi:10.1103/PhysRevC.111.034911.
- [36] U. Heinz, R. Snellings, Collective flow and viscosity in relativistic heavy-ion collisions, Ann. Rev. Nucl. Part. Sci. 63 (2013) 123–151. arXiv:1301.2826, doi:10.1146/annurev-nucl-102212-170540.
- [37] G. Giacalone, A. Mazeliauskas, S. Schlichting, Hydrodynamic attractors, initial state energy and particle production in relativistic nuclear collisions, Phys. Rev. Lett. 123 (26) (2019) 262301. arXiv:1908.02866, doi:10.1103/PhysRevLett.123.262301.
- [38] L. Du, C. Shen, S. Jeon, C. Gale, Probing initial baryon stopping and equation of state with rapidity-dependent directed flow of identified particles, Phys. Rev. C 108 (4) (2023) L041901. arXiv:2211.16408, doi:10.1103/PhysRevC.108.L041901.
- [39] L. Du, Bulk medium properties of heavy-ion collisions from the beam energy scan with a multistage hydrodynamic model, Phys. Rev. C 110 (1) (2024) 014904. arXiv:2401.00596, doi:10.1103/PhysRevC.110.014904.
- [40] B. Alver, G. Roland, Collision geometry fluctuations and triangular flow in heavy-ion collisions, Phys. Rev. C 81 (2010) 054905, [Erratum: Phys.Rev.C 82, 039903 (2010)]. arXiv:1003.0194, doi:10.1103/PhysRevC.82.039903.
- [41] F. G. Gardim, F. Grassi, M. Luzum, J.-Y. Ollitrault, Mapping the hydrodynamic response to the initial geometry in heavy-ion collisions, Phys. Rev. C 85 (2012) 024908. arXiv:1111.6538, doi:10.1103/PhysRevC.85.024908.
- [42] K. Aamodt, et al., Centrality dependence of the charged-particle multiplicity density at mid-rapidity in Pb-Pb collisions at  $\sqrt{s_{NN}} = 2.76$  TeV, Phys. Rev. Lett. 106 (2011) 032301. arXiv:1012.1657, doi:10.1103/PhysRevLett.106.032301.
- [43] K. Aamodt, et al., Higher harmonic anisotropic flow measurements of charged particles in Pb-Pb collisions at  $\sqrt{s_{NN}}=2.76$  TeV, Phys. Rev. Lett. 107 (2011) 032301. arXiv:1105.3865, doi:10.1103/PhysRevLett.107.032301.
- [44] C. E. Rasmussen, C. K. I. Williams, Gaussian Processes for Machine Learning, The MIT Press, 2005. doi:10.7551/mitpress/3206.001.0001.
- [45] S. Kullback, R. A. Leibler, On information and sufficiency, The annals of mathematical statistics 22 (1) (1951) 79–86.
- [46] J. H. Putschke, et al., The JETSCAPE framework arXiv:1903.07706.